

Controlling interactions between highly magnetic atoms with Feshbach resonances

This content has been downloaded from IOPscience. Please scroll down to see the full text.

2014 Rep. Prog. Phys. 77 093901

(<http://iopscience.iop.org/0034-4885/77/9/093901>)

View [the table of contents for this issue](#), or go to the [journal homepage](#) for more

Download details:

IP Address: 129.6.107.43

This content was downloaded on 03/10/2014 at 19:19

Please note that [terms and conditions apply](#).

Report on Progress

Controlling interactions between highly magnetic atoms with Feshbach resonances

Svetlana Kotochigova

Department of Physics, Temple University, Philadelphia, PA 19122, USA

E-mail: skotoch@temple.edu

Received 22 January 2014, revised 14 April 2014

Accepted for publication 3 June 2014

Published 15 September 2014

Abstract

This paper reviews current experimental and theoretical progress in the study of dipolar quantum gases of ground and meta-stable atoms with a large magnetic moment. We emphasize the anisotropic nature of Feshbach resonances due to coupling to fast-rotating resonant molecular states in ultracold s-wave collisions between magnetic atoms in external magnetic fields. The dramatic differences in the distribution of resonances of magnetic $^7\text{S}_3$ chromium and magnetic lanthanide atoms with a submerged 4f shell and non-zero electron angular momentum is analyzed. We focus on dysprosium and erbium as important experimental advances have been recently made to cool and create quantum-degenerate gases for these atoms. Finally, we describe progress in locating resonances in collisions of meta-stable magnetic atoms in electronic P-states with ground-state atoms, where an interplay between collisional anisotropies and spin-orbit coupling exists.

Keywords: ultracold collisions, magnetic atoms, Feshbach resonances, quantum gasses, dipole-dipole interactions, anisotropic interactions

(Some figures may appear in colour only in the online journal)

1. Introduction

Breakthroughs in the experimental realization of ultracold dipolar quantum gases of atoms with a large magnetic moment, such as Cr [1], Dy [2, 3] and Er [4, 5], have opened a new scientific playground for the study of strongly correlated atomic systems. These breakthroughs are not only limited to ground-state atoms, but apply also to meta-stable P-state systems, where the non-zero orbital angular momentum contributes to a substantial magnetic moment [6, 7]. This new research area is enabled by the long-range and anisotropic nature of the magnetic dipole-dipole interactions between magnetic atoms that allow one to engineer exotic many-body phases with control and tunability [8, 9]. Due to their large spin, dipolar gases of magnetic atoms represent an excellent environment for exploring the interface between condensed matter and atomic physics, as recently illustrated by [10], where a complex spin dynamics is observed for doubly occupied sites of an optical lattice containing Cr atoms. In

addition, ultracold samples of magnetic atoms are proposed for precision measurements of parity nonconservation and variation of fundamental constants [11, 12], as well as quantum information processing [13]. For example, robust quantum memory can be created with highly magnetic atoms coupled to a super-conducting stripline [14].

1.1. Characterization of Feshbach resonance

In this review we will explore the concept of controlling the interactions between ultracold magnetic atoms with magnetic Feshbach resonances. The limit of infinitely strong interactions between atoms leads to strongly interacting quantum gases. Alternatively, interactions can be turned to zero to create an ideal Fermi or Bose gas.

Figure 1(a) illustrates the physics of a Feshbach resonance based on a schematic picture of the interaction potentials between two atoms. Typically, in ultracold-atom experiments a homogeneous magnetic field B is present and all atoms are

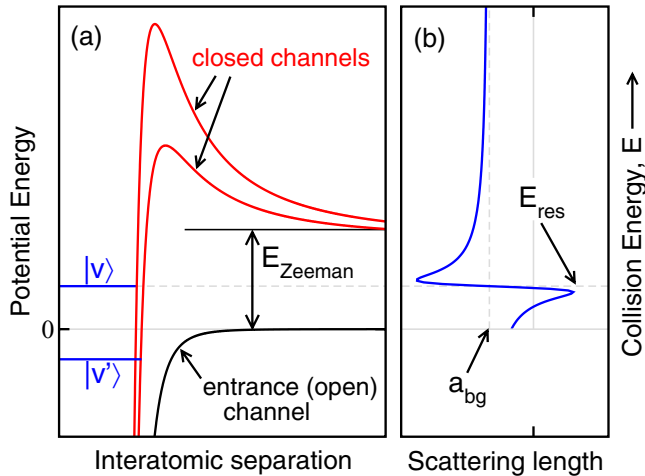


Figure 1. (a) Schematic of interatomic potentials of magnetic atoms. Scattering starts in the entrance and open s-wave channel. A Feshbach resonance is due to a bound state $|v\rangle$ of a potential of a closed channel with a dissociation energy above that of the open channel. Here, the splitting, E_{Zeeman} , is due to the Zeeman interaction and can be varied with a magnetic field. The vibrational level $|v'\rangle$ of a second closed channel is a stable and weakly bound molecular level and can become a resonance when E_{Zeeman} is further increased. (b) shows the scattering length as a function of collision energy. A resonance with a distinctive Fano profile [15] occurs near energy E_{res} .

prepared in its energetically lowest Zeeman sublevel. Two such atoms form the entrance or open channel. Closed channels correspond to pairs of atoms in energetically higher Zeeman states. By changing the magnetic field strength the closed channel energy shifts with respect to open channel energy.

In the course of the collision the open and closed channels couple and a magnetic Feshbach resonance appears, when a bound state of a closed channel has an energy near the collision energy of the open channel. The bound state is resonantly coupled to the continuum. As we will discuss below in more detail for collisions of magnetic atoms, coupling between open and closed channels can only occur due to anisotropic molecular interactions whose strengths depend on the direction along which the atoms approach each other. Then for an entrance channel with no relative orbital angular momentum ℓ , an s-wave channel, coupling occurs only to closed channels with non-zero partial wave. As shown in figure 1(a) a non-zero partial wave leads to a centrifugal barrier for the closed channel potentials.

Figure 1(b) shows the scattering length, a , as a function of collision energy E in the presence of a Feshbach resonance with resonance energy E_{res} . The (s-wave) scattering length is a convenient measure of the strength of the atom–atom interactions at small collision energies. In the limit of zero collision energy the total elastic cross-section $\sigma = 4\pi a^2$. Quantum mechanics allows a to be either positive or negative. Moreover, the scattering length can depend on collision energy as shown in figure 1(b) by a distinctive Fano profile for $E \approx E_{\text{res}}$. Away from the resonance the scattering length approaches a background value.

Figure 2 gives a second view of the magnetic Feshbach resonance. In this figure the scattering length is shown as

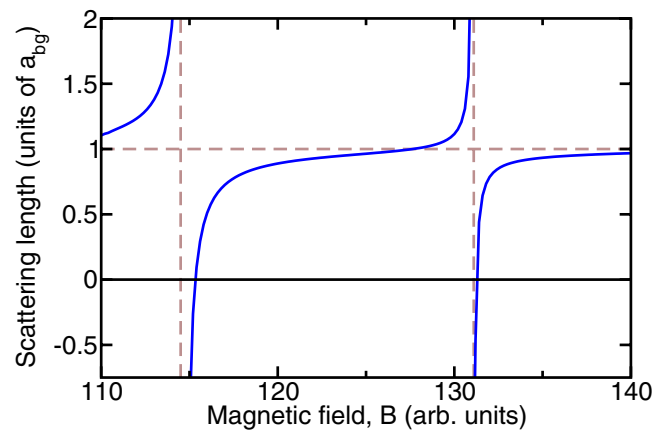


Figure 2. Example of a scattering length at zero collision energy as a function of magnetic field. The figure shows two resonances, one broader than the other, over a small magnetic field region (in arb. units). The scattering length is scaled in units of the positive background value, a_{bg} , away from both resonances.

a function of magnetic field for zero collision energy. A resonance occurs whenever the scattering length or effective size of the atom goes through infinity. The analytic form for an individual resonance at zero collision energy was derived in [16] and given by

$$a(B) = a_{\text{bg}} \left(1 - \frac{\Delta}{B - B_{\text{res}}} \right),$$

where a_{bg} is the background scattering length, B_{res} is the magnetic field position of the resonance, and Δ is the magnetic width. In fact, it can also be shown that over a sufficiently small magnetic field range $E_{\text{res}}(B) = \mu_{\text{res}}(B - B_{\text{res}})$, where μ_{res} is the magnetic moment difference of the resonant bound state and the open channel.

1.2. Role of Feshbach resonances in ultracold collisions

The crucial role that magnetic Feshbach resonances play can be understood from typical densities and temperatures of dilute quantum gases in weak (harmonic) dipole traps created by focused laser beams. The density for the dilute ultracold gas of atoms varies from $n = 10^{12}$ to 10^{15} atoms cm^{-3} , which gives a mean interparticle separation of around 100 nm. The temperatures are within 1 nK to 1 μK corresponding to de Broglie wavelengths Λ_{dB} of order of the mean separation. At phase space densities $n\Lambda_{\text{dB}}^3$ of order one a gas of bosonic atoms forms a Bose–Einstein condensate (BEC). At the same time the background s-wave scattering length is of order 5 nm, much smaller than the average separation between the atoms. It can be tuned via magnetic Feshbach resonances, to much larger values leading to strongly interacting quantum gases.

It is also worth noting that typical Zeeman energies, E_{Zeeman} , are of order $k_{\text{B}} \times 100 \mu\text{K}$ for a magnetic field strength of order 1 G. Here k_{B} is the Boltzmann constant. Only for much weaker magnetic fields is the Zeeman energy of the order of typical temperatures. Magnetic fields of order 10^3 G are routinely created. The same analysis shows that for a 1 G change in the magnetic field the resonance energy $E_{\text{res}}(B)$ can change by $k_{\text{B}} \times 100 \mu\text{K}$.

Feshbach resonances play a much larger role than just being able to enhance the interaction strength. They are also used to create a BEC of weakly bound molecules [17]. One such bound state is shown as level $|v'\rangle$ in figure 1. This bound state can be further stabilized by conversion to a deeply bound molecule by two- or more-photon Raman transitions [18, 19]. Finally, three-body Efimov physics [20] can be explored.

1.3. Short history

The first theoretical prediction of Feshbach resonances in collisions of ultracold cesium atoms was published by Tiesinga *et al* in 1993 [21], while the first observation of a Feshbach resonance in ultracold collisions of sodium atoms was published by Ketterle's group in 1997 [22]. The impact of Feshbach resonances in quantum degenerate alkali-metal gases has been broadly discussed over the past two decades. Theoretical concepts of the production of cold molecules via magnetically tunable Feshbach resonances were presented in [17]. It was followed by an extensive review [23] that focused on Feshbach resonances as the essential tool to control the interactions between ultracold alkali-metal atoms. This included a discussion of a numerous experimental methods to detect resonances as well as a discussion of their applications. Reference [23] also provided a description of the early history behind the phenomenon of resonant coupling between a bound state and a continuum and the observation of asymmetric Fano profiles [15] due to quantum interference in photo-ionization and absorption spectra. An excellent review on recent advances on Bose-condensed quantum gasses of ultracold dipolar atoms and molecules can be found in [24].

1.4. Anisotropic nature of Feshbach resonances

In this review we explore the anisotropic nature of Feshbach resonances in the collision between ultracold highly magnetic atoms. Highly magnetic atoms are atoms with an electronic ground state which has a large total angular momentum \vec{j} and thus a large magnetic moment $g\mu_B j$, where g is the atomic g factor and μ_B the Bohr magneton. Examples of such atoms are chromium and the lanthanides erbium and dysprosium with an angular momentum $j = 3, 6,$ and $8,$ respectively. In addition, we will describe recent efforts to observe anisotropic resonances in collision of meta-stable atoms with non-zero electronic orbital angular momentum L . We will contrast such resonances with those observed in alkali-metal atom collisions, where the broadest (strongest) Feshbach resonances are hyperfine induced and the resonant bound states do not rotate.

Atoms have a large magnetic moment when several of the electrons in open electron shells are aligned, either via their spin or their orbital angular momentum. In chromium the magnetic moment is solely due to the alignment of the spin of the six electrons in the open $3d^5$ and $4s$ shells. Their total orbital electron wavefunction is spherical (an S state). The most intriguing magnetic atoms are the submerged-shell lanthanide atoms. They have an electronic configuration with an open inner $4f$ shell shielded by a closed outer $6s^2$ shell. Their magnetic moment is also due to alignment of electron orbital

angular momenta so that the orbital electron wavefunction becomes non-spherical.

Interactions between magnetic atoms are orientation dependent or anisotropic. At room temperature anisotropic interactions are much smaller than kinetic energies and other major interactions between the atoms and, therefore, can be ignored. The situation is different for an ultracold gas. Reference [25], for example, demonstrated that the anisotropy due to the magnetic dipole-dipole interaction between ultracold chromium atoms leads to an anisotropic deformation of a Bose condensate. Furthermore, there is a strong evidence that anisotropy plays a dominant role in collisional relaxation of ultracold atoms with large magnetic moments [26–32].

The density of Feshbach resonances as a function of magnetic field is for some highly magnetic atomic species so high that statistical interpretations of the resonance spectrum become necessary. Originally, such statistical theories described level distribution in nuclear physics [33, 34], or Rydberg levels in spatial-dependent magnetic fields [35].

The remaining part of this review is set up as follows. In section 2 we start by describing the long-range interatomic interactions that control the origin of the Feshbach resonances. We focus in particular on the interplay between the isotropic and anisotropic interactions. In section 3 we describe the role of anisotropic dipolar interactions on Feshbach resonances in the collisions of atomic chromium. We also describe some of the applications of resonances in the context of many-body physics. Feshbach resonances in magnetic lanthanide-atom collisions are non-perturbative in the anisotropic interactions and will be discussed in section 4 for dysprosium and erbium. For erbium resonances the connection to statistical interpretations of resonance locations will be established as well. Resonances in collisions between atoms in meta-stable states will be discussed in section 5. We conclude in section 6.

2. Basic physics of atomic interactions

2.1. Isotropic interactions

Most current ultracold-atom experiments use alkali-metal atom gases, which have only one open valence electron shell. In fact, this shell is an s orbital containing one electron. The bond between atoms with such valence configuration is isotropic. Additionally, for internuclear separations R , where the atomic electron clouds do not significantly overlap, this bond is characterized by the isotropic van der Waals interaction

$$V(\vec{R}) \rightarrow \frac{C_6^{\text{iso}}}{R^6} \quad \text{for } R \rightarrow \infty,$$

where C_6^{iso} is the isotropic van der Waals coefficient. Moreover, it was quickly realized that as this interaction energy decays relatively fast with R the complete potential, both short and long-range, for many purposes, such as the modeling of quantum degenerate gases, can be replaced by a contact delta-function interaction

$$V_{\text{delta}}(\vec{R}) = g_0 \delta(\vec{R}) \frac{\partial}{\partial R} R,$$

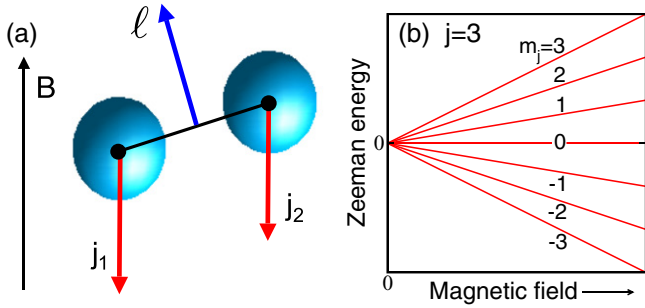


Figure 3. (a) A schematic of the angular momenta to describe the collision between bosonic magnetic atoms. (b) The Zeeman energy of the magnetic sublevels of a spin-3 magnetic atom as a function of field strength.

with strength g_0 . This interaction again does not depend on the angle of approach and is thus isotropic. Its strength is chosen in such a way that both potentials, $V(\vec{R})$ and $V_{\text{delta}}(\vec{R})$, have the same scattering phase shift $\eta(k) \rightarrow -a_s k$ for ultracold collision energies E , where a_s is the s-wave scattering length and wave number k is defined by $E = \hbar^2 k^2 / (2\mu_r)$. This then leads to $g_0 = (2\pi\hbar^2 / \mu_r) \times a_s$ and μ_r is the reduced mass of the atom pair.

2.2. Anisotropic interaction

In contrast, interactions between atoms with a large permanent magnetic dipole moment are controlled by anisotropic forces. This anisotropy is present at both short and long-range interatomic separations, but is most easily explained for large separations in terms of the three contributing forces. They are the magnetic dipole–dipole $V_{\mu\mu}(\vec{R})$, van der Waals dispersion $V_{\text{vdW}}(\vec{R})$, and quadrupole–quadrupole $V_{QQ}(\vec{R})$ interaction potentials, respectively. (For details on the short-range potentials see [36].)

The natural starting point for a collision of bosonic magnetic atoms in a magnetic field are the orthonormal basis states $|j_1 m_1\rangle |j_2 m_2\rangle Y_{\ell m}(\theta, \phi)$, where the kets $|j_i m_i\rangle$ are the electronic wavefunctions of atom $i = 1, 2$ with total atomic angular momentum \vec{j}_i and projection m_i along the direction of the magnetic field. The spherical harmonics $Y_{\ell m}(\theta, \phi)$ describe the rotational wavefunction of the two atoms, where the angles θ and ϕ orient the internuclear axis relative to the magnetic field direction and $\vec{\ell}$ is the relative orbital angular momentum (also known as the partial wave). Note that when both bosonic atoms are prepared in the same spin state, only channels with even values of ℓ are allowed. Figure 3 shows a schematic picture of these angular momenta as well as the linear-dependence of the Zeeman energy of the atomic sublevels in a magnetic field.

2.3. Theoretical background for interactions between magnetic atoms

The three long-range interactions can be systematically represented in terms of tensor operators that describe the coupling between the three angular momenta \vec{j}_1 , \vec{j}_2 , and $\vec{\ell}$.

Following [36] we have

$$V_{\mu\mu}(\vec{R}) = \frac{c_{\mu\mu}}{R^3} \sum_q (-1)^q C_{2,-q}(\theta, \phi) T_{2q}^{(2)}, \quad (1)$$

$$V_{\text{vdW}}(\vec{R}) = - \sum_{k=0,2,4;i} \frac{c_k^{(i)}}{R^6} \sum_q (-1)^q C_{k,-q}(\theta, \phi) T_{kq}^{(i)}, \quad (2)$$

and

$$V_{QQ}(\vec{R}) = \frac{c_{QQ}}{R^5} \sum_q (-1)^q C_{4,-q}(\theta, \phi) T_{4q}^{(1)}, \quad (3)$$

where operators $C_{kq}(\theta, \phi) = \sqrt{4\pi/(2k+1)} Y_{kq}(\theta, \phi)$ mix different partial waves ℓ . (Examples of this function are $C_{00}(\theta, \phi) = 1$ and $C_{20}(\theta, \phi) = (3 \cos^2 \theta - 1)/2$.) The spherical tensor operators $T_{kq}^{(i)}$ of rank k and component q describe couplings between the atomic angular momenta \vec{j}_1 and \vec{j}_2 and are given by

$$T_{00}^{(1)} = I, \quad T_{00}^{(2)} = [j_1 \otimes j_2]_{00}, \quad T_{2q}^{(2)} = [j_1 \otimes j_2]_{2q}, \quad (4)$$

and

$$T_{2q}^{(1)} = [j_1 \otimes j_1]_{2q} + [j_2 \otimes j_2]_{2q}, \quad (5)$$

$$T_{4q}^{(1)} = [[j_1 \otimes j_1]_2 \otimes [j_2 \otimes j_2]_2]_{4q},$$

$$T_{2q}^{(3)} = [[j_1 \otimes j_1]_2 \otimes [j_2 \otimes j_2]_2]_{2q},$$

$$T_{00}^{(3)} = [[j_1 \otimes j_1]_2 \otimes [j_2 \otimes j_2]_2]_{00},$$

where I is the identity operator and $[j_1 \otimes j_2]_{kq}$ denotes a tensor product of angular momentum operators \vec{j}_1 and \vec{j}_2 of atoms 1 and 2 coupled to an operator of rank k and component q [37]. The higher-order tensor operators are constructed in an analogous manner. The coefficients $c_{\mu\mu}$, c_{QQ} , and $c_k^{(i)}$ are the strengths of the individual terms.

Many of the tensor operators in equations (1)–(3) have a straight forward interpretation. Firstly, a contribution is anisotropic when it contains a $C_{kq}(\theta, \phi)$ with non-zero rank k . Moreover, to first-order perturbation theory in the interactions, the projections m_1 , m_2 , and m and partial wave ℓ can change up to 2 units due to the magnetic dipole interaction and up to 4 units due to the quadrupole–quadrupole interaction and the anisotropic dispersion potential [37].

The van der Waals dispersion interaction in equation (2) contains multiple contributions. The largest by far is the isotropic and spin-independent term proportional to the identity operator. The term with $T_{00}^{(2)}$ or equivalently proportional to $\vec{j}_1 \cdot \vec{j}_2$ induces spin–spin coupling without affecting the relative orbital angular momentum. The dispersion term proportional to $T_{2q}^{(2)}$ in equation (4) can be recognized as describing the same coupling between angular momenta as the magnetic dipole–dipole interaction. The van der Waals contribution, however, decays as $\propto 1/R^6$.

Equation (5) defines four more tensors $T_{kq}^{(i)}$. Each is connected to a term of the dispersion potential and is extremely relevant for the interactions between the Dy and Er lanthanide atoms. In fact, [36] showed that, after the term proportional to the spin-independent $T_{00}^{(2)}$, the largest dispersion term is the one proportional to $T_{2q}^{(1)}$. It corresponds to coupling of the quadrupole moment operator $[j_i \otimes j_i]_{2q}$ of atom i to the rotation

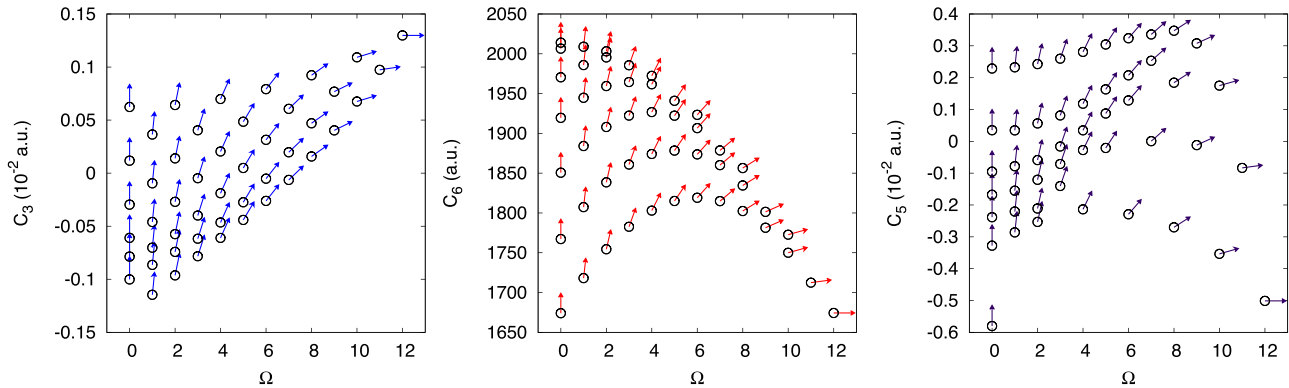


Figure 4. From left to right the *gerade* adiabatic C_3 , C_6 and C_5 coefficients in atomic units for the interaction between two ground state $^3H_{j=6}$ Er atoms as a function of the projection Ω of the total angular momentum \vec{J} on the interatomic axis. For each Ω there are approximately $(12 - |\Omega|)/2$ *gerade* adiabatic coefficients. Since interactions between atoms are orientation dependent, the arrows on the graph symbolize the anisotropy of the interactions.

of the molecule. For atomic chromium with its spherical electron wavefunction anisotropic dispersion and quadrupole–quadrupole interactions are zero leaving only the magnetic dipole–dipole interaction as an anisotropic interaction.

This description of collisions and interactions between magnetic atoms in terms of tensor operators should be compared to that of collisions between alkali-metal atoms [17]. Alkali-metal atoms have a non-zero nuclear spin \vec{i} and, in addition to the Zeeman interaction, an atomic hyperfine coupling between electron and nuclear spin $\propto (\vec{j} \cdot \vec{i})$ must be included. On the other hand, as remarked upon at the beginning of this section, the bond is isotropic with a van der Waals potential that is fully given by the simplest tensor $-c_0^{(1)}C_{00}(\theta, \phi)T_{00}^{(1)}/R^6 = -c_0^{(1)}/R^6$. The short-range potentials can be succinctly described by $V_{\text{exch}}(R)(\vec{j}_1 \cdot \vec{j}_2)$, where $V_{\text{exch}}(R)$ is the so-called exchange potential, which is an exponentially decaying function of R . The alkali-metal atoms do have a magnetic moment, but their magnetic dipole–dipole interaction is weak.

2.4. Relative size of anisotropic interactions

An elegant means to represent the character of the anisotropy of the magnetic dipole–dipole, dispersion, and quadrupole–quadrupole interactions is to diagonalize each of equations (1), (2), and (3) in the coupled molecular basis $|j_1, j_2\rangle J\Omega$ with projection Ω of $\vec{J} = \vec{j}_1 + \vec{j}_2$ along the internuclear axis. This omits couplings between different projections Ω due to the rotation of molecule. Figure 4 shows the resulting eigenvalues (multiplied by R^n with $n = 3, 5$, or 6 , respectively) or adiabatic coefficients as a function of Ω for two erbium atoms, based on values for $c_{\mu\mu}$, $c_k^{(i)}$, and c_{QQ} from [38]. (The authors used experimental data on atomic transition frequencies and oscillator strengths [39, 40] and an Er quadrupole moment of 0.029 a.u.)

Figure 4 shows that the adiabatic coefficients of the three types of interactions have a unique dependence with Ω . The values for the dipole–dipole and quadrupole–quadrupole interaction are both positive or negative reflecting the repulsive or attractive nature of these interactions depending on the direction at which atoms approach each other. The adiabatic van

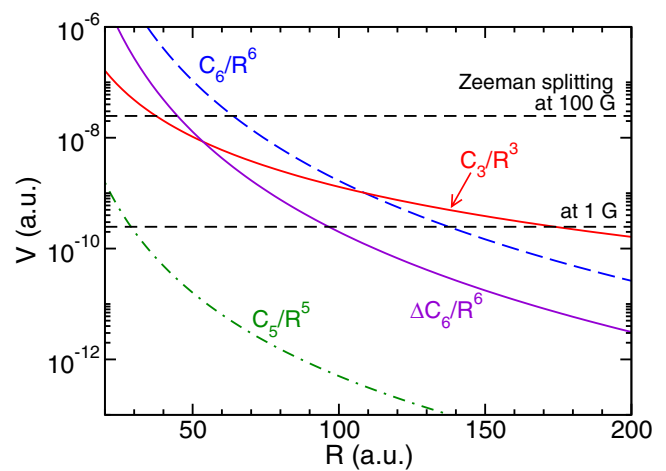


Figure 5. Typical long-range interaction potentials and Zeeman level splittings for Er+Er as a function of interatomic separation in atomic units. We have used an isotropic $C_6 = 1723$ a.u. and a ‘mean’ anisotropic $\Delta C_6 = 350$ a.u. based on figure 4.

der Waals coefficients C_6 are always positive corresponding to predominantly attractive Born–Oppenheimer potentials where a larger C_6 value implies a deeper potential. Moreover, they show a smooth nearly parabolic dependence on Ω , indicating that one of the rank $k = 2$ contributions to the van der Waals potential is the largest anisotropic contribution. A rank $k = 4$ contribution will lead to a quartic dependence with Ω .

To analyze the interplay between different long-range forces in collisions of Er atoms, figure 5 shows the strength of isotropic and various anisotropic potentials as a function of R . In our basis $|j_1 m_1\rangle |j_2 m_2\rangle Y_{\ell m}(\theta, \phi)$ the Zeeman interaction as well as the isotropic dispersion potential (labeled C_6/R^6) only shifts molecular levels and cannot cause inelastic transitions. The magnetic dipole–dipole interaction (C_3/R^3), the anisotropic component of the dispersion potential ($\Delta C_6/R^6$), and the negligibly small quadrupole–quadrupole interaction (C_5/R^5) lead to coupling between Zeeman sublevels.

For different interatomic separations different interactions dominate. At large R the Zeeman splitting is largest. When the curves for the magnetic dipole or anisotropic dispersion

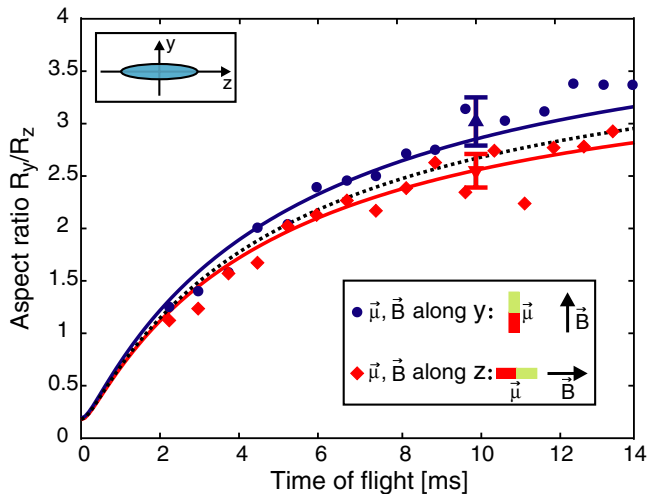


Figure 6. Aspect ratio of a freely expanding chromium BEC as a function of expansion time for two different directions of magnetization induced by a magnetic field \vec{B} (red and blue curves and markers, respectively). The markers correspond to experimental data. Dashed and solid lines correspond to a theoretical model of the expansion without and with the inclusion of the dipole–dipole interaction, respectively. Reproduced with permission from [25]. © 2005 The American Physical Society.

interaction cross the Zeeman energies m -changing collisions or relaxation can occur. For small magnetic fields the crossings occur at large interatomic separations. We also note that for $R > 60a_0$ the transitions due to the magnetic dipole–dipole interaction dominate over those of the anisotropic van der Waals interaction.

3. Feshbach tuning in collisions of atomic chromium

Over the past ten years experimental advances have led to better control of degenerate gases of magnetic ^{52}Cr atoms in the $^7\text{S}_3$ ground state. A large magnetic moment of $6\mu_B$ initiates a very strong anisotropic dipolar interaction that is 36 times stronger than that between alkali-metal atoms. Developments started at the University of Stuttgart in the group of Pfau when a BEC of Cr atoms was reported in 2005 [1]. Reference [25] demonstrated, as shown in figure 6, that by changing the direction of the magnetic field relative to the orientation of a cigar-shaped condensate, dipolar interactions modify the free expansion.

The first observation of Feshbach resonances in the collisions of ultracold bosonic ^{52}Cr atoms in the $m_j = -3$ state was reported in [41]. They found ten resonances, shown in figure 7, between $B = 4\text{ G}$ and 600 G , leading to an average density of resonances of ≈ 0.02 per Gauss. The zero nuclear spin of ^{52}Cr and, thus, the absence of a hyperfine Fermi-contact interaction allowed for an accurate model and identification of the observed resonances using multichannel scattering calculations. In fact, the average discrepancy between theoretical and experimental resonance positions is only 0.6 G . The dipole–dipole interaction was included in the theoretical modeling of [41] allowing an

accurate description of the widths of the observed resonances. A similar theoretical analysis of the Feshbach resonances observed and characterized in [41] was performed in [42].

3.1. Direct evidence for dipolar effects

Later it was shown that the effects of dipolar forces in a quantum gas of Cr can be brought out using Feshbach resonances [43]. The broadest resonances in figure 7, at $B = 589\text{ G}$, were selected for Feshbach tuning of the s -wave scattering length. With the scattering length set close to zero, direct evidence for dipolar effects on BEC was observed [44, 45]. It was shown that the magnetic dipole–dipole interaction energy can be comparable to the so-called mean-field energy. Figure 8 shows their observation of the scattering length as a function of the magnetic field near the 589 G Feshbach resonance. A characteristic anisotropic d -wave collapse and subsequent explosion, presented in [46], gave further evidence of the relevance of dipole–dipole forces.

Dipolar interactions have other consequences as well. A chromium sample prepared in the low-field seeking $m_j = +3$ state will undergo strong dipolar relaxation, where, during a collision, one or both atoms change state to a sublevel with a smaller m_j . The decrease in internal energy leads to an increased relative kinetic energy and the atoms are, typically, lost from the shallow traps in which they are held. This relaxation was observed as early as 2003 [29]. It was shown that the cross-section for relaxation scales as the cube of the magnetic dipole moment. Additional dipolar relaxation rates were measured in [47–49]. Furthermore, they showed that relaxation can be controlled by static and oscillatory magnetic fields.

Chromium atoms have also been loaded into optical lattices, periodic potential created counter-propagating laser beams. Reference [50] showed that for a one-dimensional optical lattice the stability of a pan cake-shaped dipolar ^{52}Cr condensate near $B = 589\text{ G}$ dramatically depends on the depth of the lattice. The stability measurements were performed at a magnetic field near a Feshbach resonance, where the dipole–dipole interaction dominates the short-range isotropic interactions. Another effect of a strong dipole–dipole interaction is that a gas can be stable in an optical lattice, but is not during a time-of-flight expansion after the lattice trap is turned off [51]. Non-equilibrium quantum magnetism at very small magnetic field strengths was studied by experiments in [10]. They showed that non-equilibrium spinor dynamics is modified by the non-local inter-site dipole–dipole interactions.

3.2. Cooling effect of dipolar relaxation

More recently, dipolar relaxation was used to cool a sample by adiabatic demagnetization. This cooling scheme was suggested in [52] and demonstrated experimentally in [53]. Figure 9 shows how inelastic collisions can be used to implement adiabatic demagnetization. The scheme relies on collisional relaxation in extremely small magnetic fields, where Zeeman splittings are of the order of the temperature of the gas, and on spin selection rules that can only be achieved by anisotropic interactions, where the atomic angular momentum

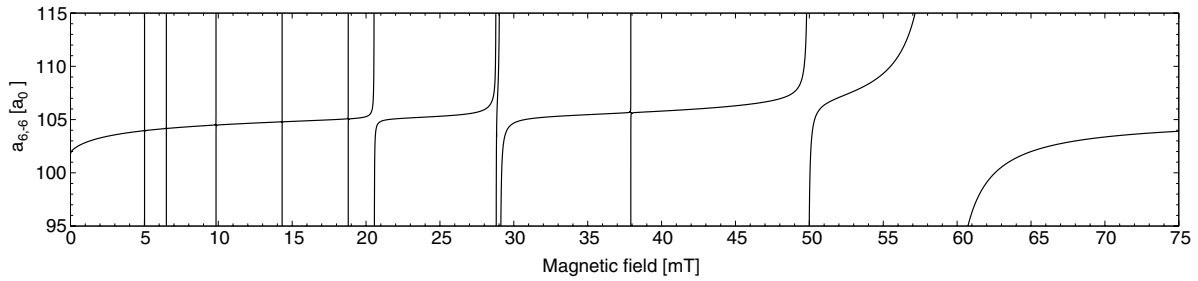


Figure 7. Calculated scattering length of two $m_j = -3$ ^{52}Cr atoms versus magnetic field where 1 mT = 10 G. Model parameters are given in [41]. See table 1 of this reference for the experimental data. Reproduced with permission from [41]. © 2005 The American Physical Society.

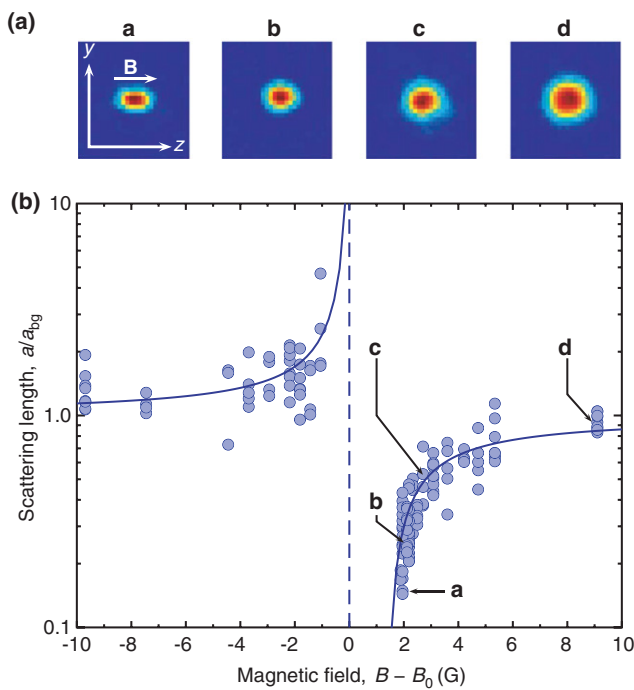


Figure 8. (a) Absorption images of a ^{52}Cr Bose condensate after expansion for four values of the magnetic field. (b) Measured scattering length of two $m_j = -3$ ^{52}Cr atoms versus magnetic field with $B_0 = 589$ G. The fields labeled a,b,c and d correspond to the four magnetic fields in (a), respectively. One clearly observes a decrease in size and increase of ellipticity when the scattering length decreases. Reproduced with permission from [44]. © 2007 Nature Publishing Group.

couples to the rotational state of the colliding atoms. Recent research [54] in demagnetization cooling of Cr atoms showed a significant improvement in efficiency over a large temperature range and for high atomic densities. The authors discuss the possibility of achieving Bose–Einstein condensation by demagnetization cooling of Dy atoms.

The role of the dipole–dipole interaction in spinor dynamics, the time evolution coherences between and populations of m_j sublevels, in a chromium BEC was explored in [55, 56]. The dynamics resembles the Einstein–de Haas effect. Anisotropic coupling transfers atoms from sublevel m_j to $m_j + 1$ leading to the generation of dynamical rotation. Reference [57] showed that the Einstein–de Haas effect is easily destroyed due to the role of Larmor precession in an external magnetic field.

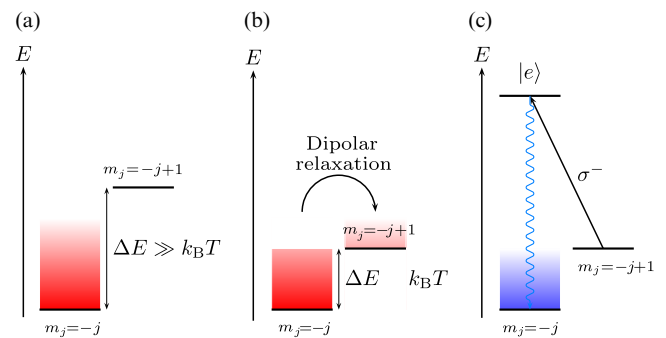


Figure 9. Principle of demagnetization cooling. (a) In a magnetic field where the Zeeman splitting ΔE between adjacent Zeeman sublevels m_j is larger than the thermal energy $k_B T$, a gas of magnetic atoms in the energetically lowest $m_j = -j$ state is stable. There are no inelastic dipolar relaxation processes. (b) By slowly reducing the field strength so that $\Delta E \approx k_B T$, the dipole–dipole induced transitions to state $m_j = -j + 1$ become allowed and kinetic energy is converted into Zeeman energy. (c) By applying an optical pumping pulse of σ^- polarized light, the cloud can again be polarized but now is at a reduced temperature. The excess Zeeman energy is taken away by the spontaneously emitted photons. The lowest achievable temperature is of the order of the photon recoil energy, the energy added by the optical pumping process. Reproduced with permission from [24]. © 2009 IOP Publishing Ltd.

In summary, the most important feature of a Cr quantum gas is a strong anisotropic dipole–dipole interaction, based on the large magnetic moment (electronic spin) of the Cr atom. These interactions lie at the heart of many fascinating effects observed or predicted for a Cr BEC.

4. Degenerate gases of dysprosium and erbium atoms

4.1. Collisional properties of submerged-shell atoms

Over the past decade significant attention has been devoted to the characterization of the interactions between submerged-shell 3d-transition-metal and 4f-rare-earth atoms [25, 28–30, 44, 58–60]. These atoms have an electronic configuration with an electron vacancy in the inner shell shielded by a closed outer shell. It was long assumed that inelastic, energy-releasing collisions of submerged-shell atoms are substantially suppressed due to shielding caused by the closed outer-shell electrons. This effect was first predicted and

demonstrated for collisions between submerged-shell atoms with helium [30, 58, 59, 61]. The suppression of inelastic loss with a cold gas of He atoms allowed for sympathetic cooling of submerged-shell atoms to millikelvin temperatures. Theoretical analyses by [62] of experimental measurements [30] explain this low rate by the fact that anisotropy in interactions between open-shell lanthanide atoms and helium is extremely small.

Measurements [27, 28, 31, 60] of the spin relaxation rates in collisions of two submerged-shell atoms, however, have shown no such suppression and, in fact, the rate coefficients are of the same order of magnitude ($10^{-10} \text{ cm}^3 \text{ s}^{-1}$) as for non-submerged-shell atoms. This implies the presence of additional spin relaxation mechanisms.

Submerged-shell atoms, such as dysprosium $\text{Dy}(^6\text{I}_8)$ and erbium $\text{Er}(^3\text{H}_6)$, focused on in this review, have not only a large magnetic moment but also a large non-zero orbital angular momentum L . The electronic structure of these non-S state atoms leads to an additional source of anisotropy in their interactions and it is, for example, of relevance to determine its effect on Feshbach resonance tuning and control.

The importance of anisotropy in the interactions of cold atoms with non-zero angular momenta was first theoretically investigated by [26, 37, 63, 64]. They have shown strong evidence of electronic interaction anisotropy as a leading spin relaxation mechanism in collisions.

4.2. Universality in collisions of Dy atoms

A wealth of fascinating properties of interacting Dy atoms in their ground state was revealed by the theoretical analyses of [32]. Using experimental data on atomic transition frequencies and oscillator strength the authors constructed 153 interaction potentials that dissociate to two ground-state atoms. Splittings between these potentials provide an estimate for the strength of the anisotropic forces that play a crucial role in the alignment of the open 4f-shell electrons and in sublevel- or m -changing relaxation mechanisms. In addition, the authors used a universal scattering model to study inelastic scattering and estimate loss rates. This model, originally developed in [65, 66], assumes scattering from a single potential $-C_6/R^6 + \hbar^2 \ell(\ell+1)/(2\mu_r R^2)$ for $R > R_c$ and where C_6 is equal to the isotropic van der Waals coefficient. Atom pairs that reach the critical interatomic separation R_c undergo m -changing collisions with unit probability independent of scattering energy and partial wave ℓ . The model assumes that for $R > R_c$ coupling due to the anisotropic dispersion potential and the dipole-dipole interaction can be neglected. Figure 10(a) shows inelastic rate coefficients for a gas of Dy atoms with equal populations in all m sublevels as a function of collisional energy within this universal model.

Another important anisotropic interaction between Dy atoms that can cause inelastic losses comes from the magnetic dipole-dipole interactions. The rate of these losses was estimated in [32] by using perturbative Born approximation and shown as a function of collision energy in figure 10(b). These rates were compared to the experimental loss rate measured at a temperature of $\approx 500 \mu\text{K}$ confined in a quadrupole magnetic

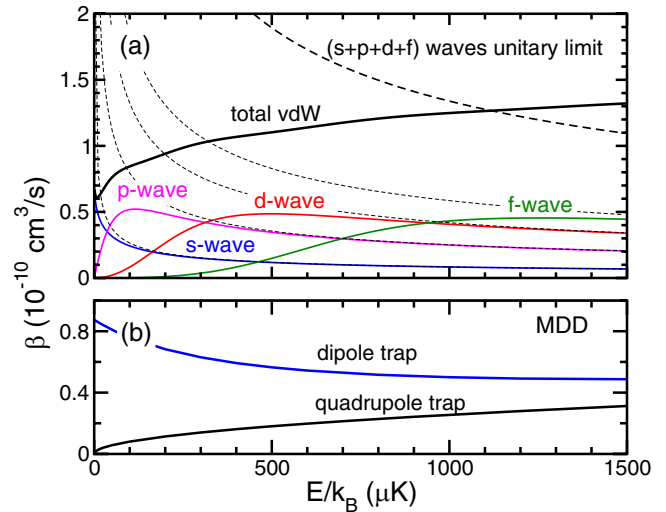


Figure 10. The inelastic loss rate coefficient for a non-spin-polarized sample of ground state ^{164}Dy atoms as a function of collision energy based on a universal scattering model for losses due to the anisotropy of the dispersion potential (a) and a Born approximation for losses from the magnetic dipole-dipole interaction (b). For the universal model rate coefficients for the lowest four partial waves and the summed rate are shown. The unitary limited rate coefficients for each of the four partial waves are plotted as dashed lines. The loss rate coefficient for the magnetic dipole-dipole interaction is given for a quadrupole as well as a dipole trap with a constant magnetic field of $B = 10 \text{ G}$. Reproduced from [32] by permission of the PCCP Owner Societies.

trap (a trap with zero magnetic field in the center) in [31]. Both experiment and theory show rates of the order of $10^{-10} \text{ cm}^3 \text{ s}^{-1}$ as predicted for other submerged-shell atoms in [28].

4.3. Quantum degenerate gas of Dy atoms

A direct and efficient transfer of atoms into an optical dipole trap allowed researchers from the University of Illinois and Stanford University to form a Bose condensate of the bosonic ^{164}Dy atoms at temperatures below 30 nK [2]. They also cooled fermionic ^{161}Dy in the presence of bosonic isotopes to form a Fermi sea of atoms thus realizing a novel, nearly quantum degenerate dipolar Bose-Fermi mixture [3].

Recent theoretical work [36] performed a fully quantum-mechanical scattering calculation of the scattering length and elastic rates between two ultracold dysprosium atoms in the lowest Zeeman sublevels $m_j = -8$ and under experimental conditions of [3]. This investigation predicted for the first time the existence of strong and broad Feshbach resonances in interaction between bosonic ^{160}Dy , ^{162}Dy , and ^{164}Dy atoms, which have zero nuclear spin, for a magnetic field range from zero to 200 G. These resonances are solely induced by the anisotropy in the long-range interaction potentials. Without the magnetic dipole-dipole and anisotropic dispersion potentials in the Hamiltonian resonances do not occur. Both anisotropies contribute to the appearance of a resonance structure. Figure 11 provides evidence of the direct effect of both anisotropies on the magnetic-field location of Feshbach resonances. Switching on and off different parts of the

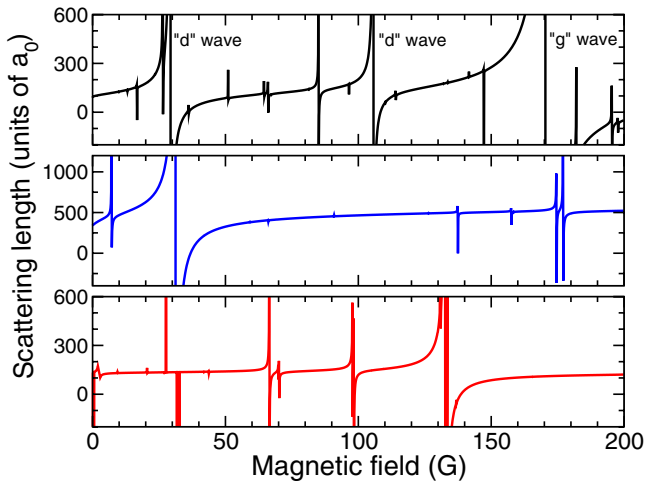


Figure 11. Predicted scattering length of $m = -8$ ^{164}Dy atoms as a function of magnetic field with and without the magnetic dipole-dipole or the anisotropic contribution of the dispersion interaction. Channels with even partial waves ℓ up to 10 are included and a collision energy $E/k_B = 30$ nK was used. The top panel shows the case when all interactions are included. For the three broad resonances the first partial wave for which the resonance appears is shown. The middle and bottom panels are obtained when the dispersion and magnetic dipole-dipole anisotropy are set to zero, respectively. Reproduced with permission from [36]. © 2012 American Physical Society.

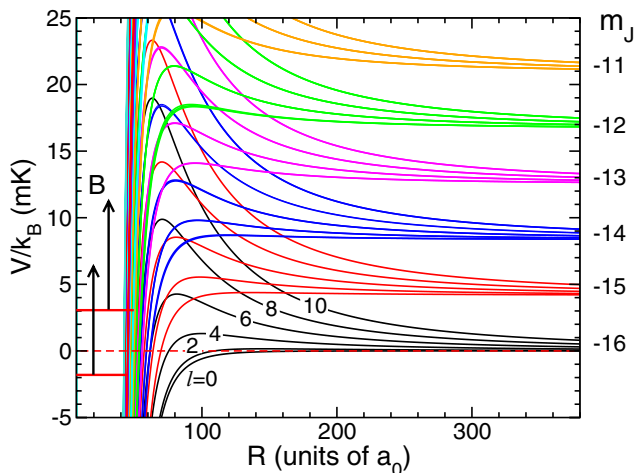


Figure 12. Potential energy curves for a $^{164}\text{Dy}+^{164}\text{Dy}$ collision for $B = 50$ G as a function of interatomic separation R . The (red) dashed line with zero energy indicates the energy of the entrance channel. The curves are colored by their $m_j = m_1 + m_2$ value, while for $m_j = -16$ curves their ℓ value is indicated. Reproduced with permission from [36]. © 2012 American Physical Society.

Hamiltonian, the researchers observed a significant change in the resonance distribution.

Despite the fact that the broadest resonances in figure 10 were identified as ‘d’- and ‘g’-wave resonance channels with ℓ up to 10 needed to be included to converge the close-coupling calculation. The long-range potential energy curves of interacting ^{164}Dy atoms for a magnetic field $B = 50$ G are shown as a function of interatomic separation in figure 12. For $R > 200a_0$ the Zeeman forces dominate the collision dynamics, whereas for $R < 200a_0$ the potential curves

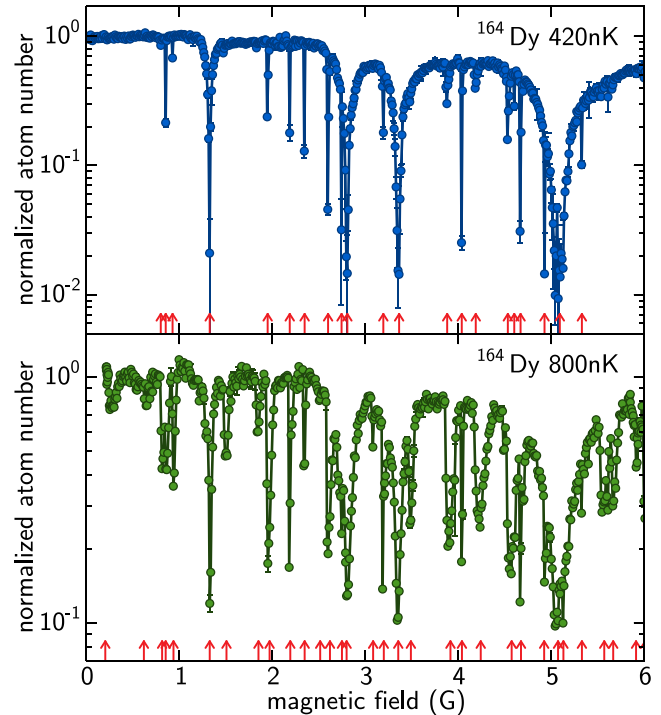


Figure 13. Experimental observation of Feshbach resonances in collisions of $m_J = -8$ ^{164}Dy atoms of [67]. The top panel shows a spectrum obtained at a temperature of ≈ 420 nK. The lower panel displays a spectrum at a higher temperature of ≈ 800 nK. The arrows indicate the positions of the resonances.

of higher partial waves overlap indicating the possibility of coupling between potentials.

4.4. First observation of low-magnetic field Feshbach resonances in Dy collisions

Reference [67] has recently reported the observation of collisional resonances in trap loss of spin-polarized Dy atoms in their energetically lowest Zeeman sublevel. The measurements were performed for three bosonic isotopes, ^{160}Dy , ^{162}Dy , and ^{164}Dy , and a single fermionic isotope of ^{161}Dy . The bosonic atoms were transferred into the $m_J = -8$ magnetic sublevel, while the fermionic atoms were placed into the lowest hyperfine sublevel $F = 21/2$, $m_F = -21/2$, where \vec{F} is the sum of the total electronic angular momentum and the nuclear spin. Observation of Feshbach resonances as shown in figure 13 was recorded in the magnetic field range from 0 to 6 G, where the resonant density exceeded 3 resonances for Gauss for bosonic ^{164}Dy at a temperature of 420 nK and about 5 resonances per Gauss for a higher temperature of 800 nK. This observation of these resonances was predicted by the simulations of [36], which showed that strong anisotropic interactions between Dy atoms will lead to the appearance of strong resonances. The theoretical calculations of the Dy Feshbach spectrum, however, were performed at a much lower collisional energy of $E/k_B = 30$ nK and exhibited a lower resonance density. In order to give quantitative insight into collisional dynamics of magnetic dysprosium the theory must optimize the model parameters and conduct calculations at the experimental conditions of [67]. It seems likely that Dy is more anisotropic

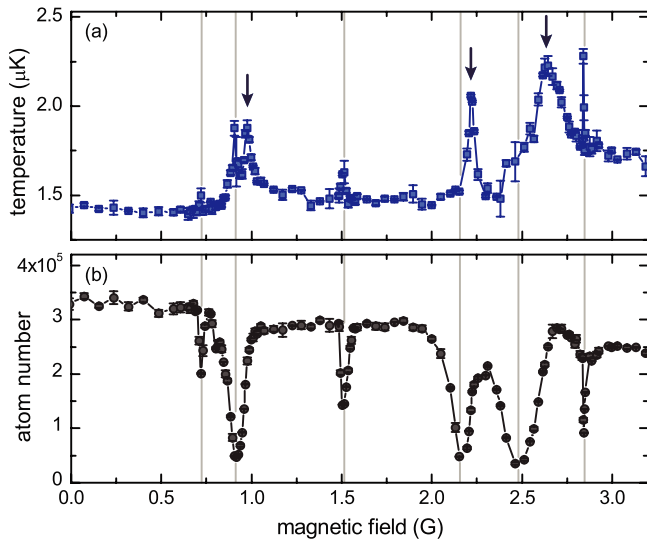


Figure 14. Experimental observation of Feshbach resonances in collisions of $m_j = -6$ ^{168}Er atoms. The measured temperature (a) and atom number (b) are plotted as a function of magnetic field. Reproduced with permission from [5]. © 2012 American Physical Society.

than previously thought [36]. In addition, at higher temperatures around 400–800 nK non-zero partial wave collisions may become important and increase the resonance density.

4.5. Study of Er atom collisions in a magneto-optical trap and an optical trap

Exploration of collisional dynamics between the ultracold erbium atoms began in 2006 with Dr McClelland’s group at NIST [68]. They demonstrated the operation of a magneto-optical trap (MOT) and laser cooling of Er to millikelvin temperatures. Later the group of Professor Ferlaino at the University of Innsbruck adapted the cooling techniques of [68] and applied a narrow-line MOT allowing them to further cool Er atoms. They reached temperatures of 15 μK [4]. After directly loading atoms into an optical dipole trap and using evaporative cooling they created a pure ^{168}Er BEC [5]. At magnetic fields below 3 G they immediately observed six Feshbach resonances as shown in figure 14. The presence of low-field resonances in the Er interactions opens extraordinary possibilities to study dipolar properties for atoms with a strong coupling between various partial waves and Zeeman sublevels.

4.6. Evidence for a strong collisional anisotropy in Er interactions

A further study by this group using high-resolution trap-loss spectroscopy [38] revealed a dense forest of Feshbach resonances for magnetic fields from 0 to 70 G. In fact, they observed for two bosonic isotopes, ^{168}Er and ^{166}Er , both in their lowest Zeeman sublevel $m_j = -6$ this unprecedented large number of resonant features with a mean density $\bar{\rho}$ of 3 resonances per Gauss. An even more dense spectrum of 26 resonances per Gauss was obtained for an optically trapped sample of fermionic ^{167}Er atoms in their lowest Zeeman sublevel, $m_F = -19/2$.

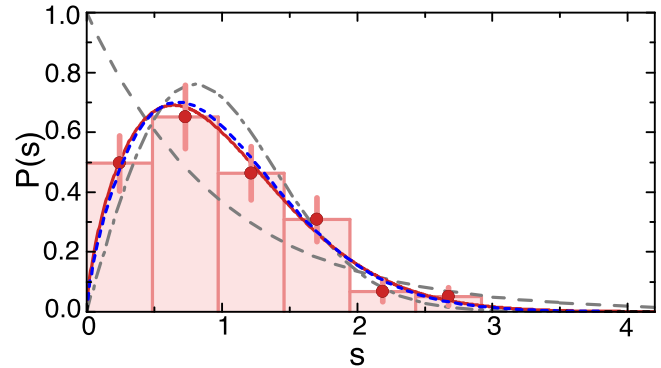


Figure 15. The normalized distribution $P(s)$ of nearest-neighbor spacings (NNS) of ^{168}Er Feshbach resonances as a function of dimensionless $s = \Delta B \bar{\rho}$, where the ΔB are NNS and $\bar{\rho}$ is the mean resonance density per unit field strength. The experimental data is shown as a bar graph and filled red circles with error bars. The dashed gray, dashed-dotted gray, and solid red curves are Poisson, Wigner–Dyson and Brody distributions fit to the experimental data, respectively. The dotted blue line is a Brody distribution fit to the distribution of NNS of a close-coupling calculation where partial waves up to $L_{\text{max}} = 20$ have been included. Reproduced with permission from [38]. © 2014 Nature Publishing Group.

Based on the enormous number of resonances the experimentalists with support of the theorists set up to investigate the statistical properties of the observed spectra for the bosonic atoms. First, the authors of [38] performed an analysis of the nearest-neighbor spacings (NNS) and interpreted their results using distributions derived in random matrix theory (RMT), originally introduced by [33, 34]. RMT attempts to characterize the presence or absence of correlations between levels or in this case Feshbach resonance positions. In parallel, several first-principle coupled-channel (cc) calculations of Er Feshbach spectra were performed. A resonance spectrum of the scattering length was obtained by only including channels with even partial waves ℓ from 0 up to L_{max} . Calculations were performed up to $L_{\text{max}} = 20$. The theoretical simulations also found a large number of resonances between $B = 0$ and 70 G, which could also be analyzed in terms of resonance distributions compared to predictions of RMT.

4.7. Statistical description of a Feshbach spectrum

Figure 15 shows the distribution of the NNS between Feshbach resonances for the ^{168}Er isotope for fields between $B = 30$ to 70 G and grouping resonance spacings ΔB in bins with a width of 160 mG. These spacings scaled to the mean spacing, s , were then fit to a Poisson distribution $P(s) = \exp(-s)$ for non-interaction levels, the Wigner–Dyson distribution $P(s) = (\pi/2)s \exp(-\pi s^2/4)$ characterizing strongly interacting levels, and the Brody distribution, which is a one-parameter function that smoothly connects between the Poisson and Wigner–Dyson distribution. The authors of [38] concluded that the NNS of erbium closely resembled a Wigner–Dyson distribution.

In addition, figure 15 shows the Brody distribution fit to the NNS of the theoretical cc spectrum with $L_{\text{max}} = 20$ and using a collision energy of $E/k_B = 360$ nK. The agreement

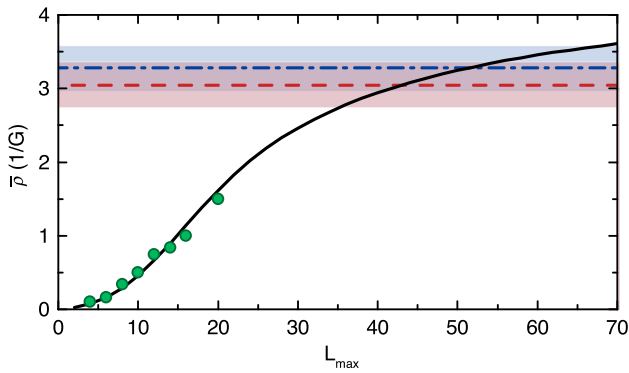


Figure 16. Mean resonance density $\bar{\rho}$ for bosonic Er as a function of the largest included partial wave L_{\max} of theoretical close-coupling calculations. The cc-calculated densities are shown by green circles up to $L_{\max} = 20$. The solid black line shows an analytical estimate of mean density for L_{\max} up to 70. The experimentally measured mean resonance densities are presented for ^{168}Er (dashed line) and for ^{166}Er (dashed-dotted line) with one sigma confidence bands (shaded areas). Reproduced with permission from [38]. © 2014 Nature Publishing Group.

between the experimental and theoretical Brody distributions is impressive. This is the more surprising as it should be noted that for $L_{\max} = 20$ the ccs calculation did not yet converge. For example the resonance density was still increasing with increasing L_{\max} and for $L_{\max} = 20$ the mean density was only $\bar{\rho} = 1.5$ per Gauss.

The behavior of the mean resonance density of Feshbach resonances obtained from cc calculations was further studied by systematically increasing the largest included partial wave L_{\max} and are shown in figure 16. The figure also shows an estimate of $\bar{\rho}$ for larger L_{\max} by essentially counting the number of weakly bound rovibrational states of the closed channels. This simple approach relied on a separation of energy scales: for small/large interatomic separations the anisotropic couplings are large/small compared to the Zeeman interaction and rotational or coriolis forces, respectively, and that, crucially, in the radial cross-over region the isotropic part of the potentials is much deeper than the Zeeman and rotational splittings. Reference [38] then concluded that at least 40 partial waves will be needed to explain the experimental resonance density.

4.8. Dipolar effects on fermionic atom cooling

We finish this section by noting that erbium has one stable fermionic isotope, ^{167}Er , with non-zero nuclear spin. First experiments for this isotope have only recently been performed. Not surprisingly the magnetic dipole-dipole interaction between these Er atoms plays a prominent role in their cooling. Reference [69] showed that fermionic atoms, all in the same magnetic sublevel, can still be thermalized even though such atoms cannot collide by even partial waves (and in particular the s-wave) as Fermi statistics forbids such channels. They must thermalize by p-wave collisions instead. This thermalization occurred with cross-sections that are consistent with perturbative predictions from universal dipole scattering theory [70, 71].

5. Magnetic control of mixed gases of ground and meta-stable rare-earth atoms

The collisional characteristics of the meta-stable $\text{Yb}^*(^3\text{P}_2)$ atoms were recently explored by Professor Takahashi's group at Kyoto University, Japan, and Professor Gupta's group at the University of Washington [6, 7]. Again in contrast to the well studied alkali-metal atom collisions, ultracold collisions between meta-stable rare-earth atoms are highly anisotropic due to the interplay between interaction anisotropies and spin-orbit coupling. The first experimental realization of optical trapping of ultracold $^{174}\text{Yb}^*(^3\text{P}_2)$ atoms and measurement of its inelastic collisional rate was performed by [72]. Fine-structure changing collisions were suggested to be the main source of these losses. Later, the same group measured the dynamic polarizability of $^3\text{P}_2$ magnetic sublevels at laser wavelengths of 532 nm [73] and 1070 nm [74] by performing a high-resolution spectroscopy in a Yb Bose condensate.

Historically, considerable attention has been given to the theory of fine-structure changing collisions of atoms in P electronic states with structureless atoms. Spin-orbit relaxation in such systems was found to be very efficient due to the interplay with interaction anisotropies. The orientation-dependent cross-section for fine-structure transitions in collisions between ground state He and ^2P Na atoms near room-temperatures was first analyzed in [75]. The oscillatory behavior of the cross-section with collision energy was shown to be related to shape resonances in the elastic scattering channels. The theory of fine-structure transitions in collisions between a proton and a fluorine atom in its ground ^2P state was formulated in terms of molecular states and treated by the quantum close-coupling method in [76].

Fine-structure changing collisions of alkaline-metal atoms in a ^3P state with He atoms were studied in [77]. They reported a significant increase in the cross-section due to orientational anisotropies leading to coriolis coupling between the orbital and electronic angular momenta. In [78] the interaction of oxygen ^3P -state atoms with the rare gases was studied. The authors found that the interaction anisotropy increases from He to Xe due to an increasing contribution from the excited ionic states. This investigation emphasized the effect of anisotropy in the van der Waals interaction on collisional dynamics of the open shell atoms. Collisions between two ^3P oxygen atoms were studied in [79]. As in previous calculations the authors estimate the cross-section of a fine-structure transition using a full quantum close-coupling theory. They found that inclusion of the fine-structure splitting in the model has a dramatic effect on the transition cross-section. In 2008 a combined experimental and theoretical study [80] of cold 1 K collisions between open P-shell bismuth and helium atoms in the presence of a magnetic field demonstrated strong Zeeman relaxation attributed to the combined effect of interaction anisotropy and spin-orbit coupling.

Finally, we note that anisotropies in atom-molecule van der Waals complexes containing P-state systems were studied in [81, 82]. It was emphasized that the long-range intermolecular forces have a significant influence on the collisional dynamics by orienting the reactants during the

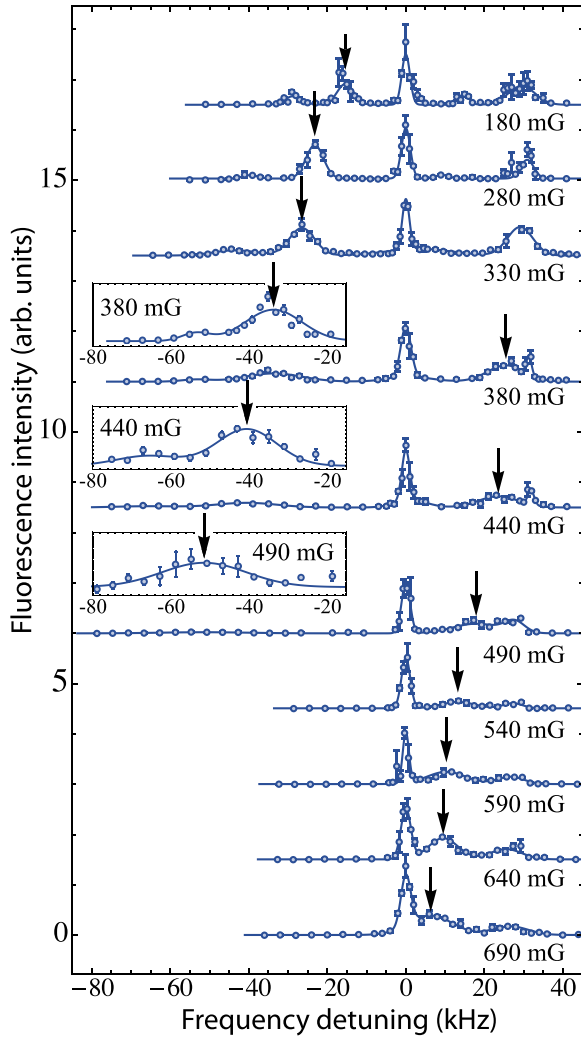


Figure 17. Excitation spectra near the 3P_2 ($m_J = +2$) state of ^{174}Yb in an optical lattice at various magnetic fields below 1 G. Lattice sites contain either one or two atoms. Peaks due to doubly occupied sites are indicated by arrows and change their location as a function of magnetic field. Reproduced with permission from [6]. © 2013 American Physical Society.

collision. In addition, spin–orbit couplings have a strong effect on the long-range forces.

5.1. Homonuclear ground and meta-stable state collisions

Feshbach resonances in ultracold meta-stable atom collisions are a result of strong interaction anisotropies that depend on the orientation of the interatomic axis relative to an external magnetic field. Resonances of this nature were recently observed by [6] for homonuclear collisions between a ground and a meta-stable 3P_2 ^{174}Yb atom held in doubly occupied sites of an optical lattice as shown in figure 17 for magnetic fields below 1 G. The spectra in figure 17 were obtained by photoassociative spectroscopy near the atomic 1S_0 - 3P_2 ($m_J = +2$) transition. The authors infer that a resonance occurs at $B_{\text{res}} = 360 \pm 10$ mG. Reference [6] also observed a Feshbach resonance in the 1S_0 - 3P_2 ($m_J = -2$) collision of the ^{170}Yb isotope. Its location is $B_{\text{res}} = 1.12 \pm 0.01$ G.

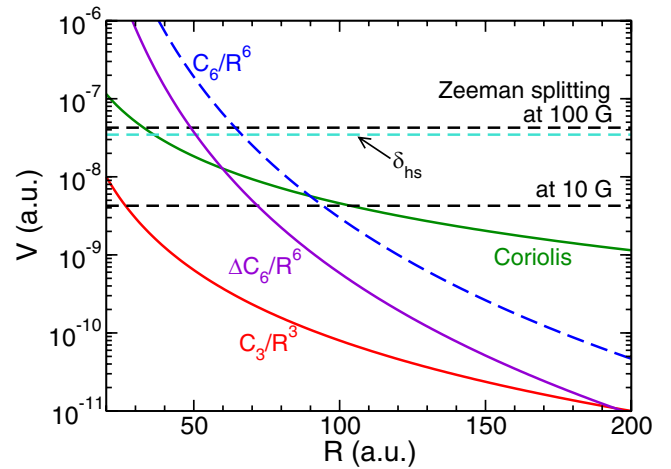


Figure 18. Splittings in the $\text{Li}+\text{Yb}^*(^3P_2)$ interaction potentials in atomic units as a function of interatomic separation. The Zeeman splitting is $(g_{\text{Li}} + g_{\text{Yb}^*})\mu_B B$, δ_{hs} corresponds to the hyperfine splitting of the ground state of Li, the coriolis interaction is $\hbar^2/(2\mu_r R^2)$, the magnetic dipole–dipole interaction is C_3/R^3 , and the isotropic and anisotropic dispersion interaction is C_6/R^6 and $\Delta C_6/R^6$, respectively. Here $g_{\text{Li}} = 2$ and $g_{\text{Yb}^*} = 1.5$ are g-factors of Li and $\text{Yb}^*(^3P_2)$, respectively. We assumed $C_6 = 2987.5$ a.u. and $\Delta C_6 = 585$ a.u. [7].

5.2. Heteronuclear alkali-metal and meta-stable rare-earth collisions

In 2011 a quantum-degenerate mixture of fermionic alkali-metal ^6Li and bosonic ^{174}Yb atoms was obtained by Dr Gupta’s group [83] with the goal to use photoassociation to create paramagnetic polar LiYb molecules. Now this group has reported on the realization of an ultracold mixture of ^6Li and meta-stable $^{174}\text{Yb}^*(^3P_2)$ [7]. Measurements of the two-body inelastic decay coefficients for collisions of the 3P_2 $m_J = -1$ Zeeman sublevel and a ground state Li atom indicate a low rate coefficient of the order of $10^{-12} \text{ cm}^3 \text{ s}^{-1}$. As an important aside the authors of [7] also calculated the dynamic polarizability of the ground and meta-stable Yb^* state over a wide range of laser frequencies allowing the future identification of magic frequencies where both states are identically trapped. The long-range dispersion coefficients were also evaluated. Based on these analyses figure 18 shows the strength of the two major anisotropic long-range interatomic interactions and compares them to Zeeman energies and the hyperfine splitting of the Li ground state. When the curves for the magnetic dipole or anisotropic dispersion interaction cross the Zeeman, hyperfine, and/or rotational energies spin flips can occur. The magnetic dipole–dipole potential crosses the Zeeman curves for $B = 10$ and 100 G at $R < 50a_0$, where chemical bonding should play an important role as well.

5.3. Prediction of anisotropy-induced resonances in mixed species collisions

An important step in the conversion of a weakly interacting gas of ^6Li and ^{174}Yb atoms into a strongly interacting one, or even to a gas of weakly bound molecules, is magnetic Feshbach tuning. Theoretical work of [84] on ground-state collisions of ^6Li and ^{174}Yb recently predicted that magnetically tunable

Feshbach resonances can exist due to a modification of the Li hyperfine coupling in the presence of the Yb atom. However, these resonances are expected to be extremely narrow, on the order of mG, and difficult to observe. A promising alternative way to observe broader and stronger magnetic Feshbach resonances is to consider interactions between a ground-state Li atom and a long-lived meta-stable Yb atom. These meta-stable Feshbach resonances and their associated weakly bound meta-stable molecules might be used to efficiently transfer colliding atoms to a vibrational level of the absolute molecular ground state.

Reference [85] performed cc calculations for ${}^6\text{Li}+{}^{174}\text{Yb}^*({}^3\text{P}_2)$ meta-stable collisions as a function of magnetic field and showed that broad and strong magnetic Feshbach resonances can be formed as the meta-stable $\text{Yb}^*({}^3\text{P}_2)$ atom has non-zero electron orbital angular momentum \vec{L} and, thus, their interactions are highly anisotropic. The predicted meta-stable magnetic Feshbach resonances [85] may become vulnerable to decay processes or broadening mechanisms that render them unobservable, such as the spin-orbit interaction of the meta-stable Yb^* atom. Collisional resonances of the LiYb^* system could also be broadened by R -dependent spontaneous emission of the interacting atoms. This process occurs as excited short-lived lithium states contribute to the formation of the molecular bond. For the future it would be beneficial to determine resonance broadening due to this effect.

6. Conclusion

This paper has discussed recent advances in our understanding of scattering properties of high-spin open-shell atomic systems. In particular, our attention was directed toward magnetic atoms with submerged inner shells, such as chromium, dysprosium and erbium, in their ground state as well as ytterbium in its meta-stable state. These atoms, both bosons and fermions, were successfully cooled to quantum degeneracy and confined in optical dipole traps or optical lattices, allowing the study of their collisions at the quantum level.

Similar to alkali-metal atom collisions, magnetic Feshbach resonances represent a powerful tool to control the interactions between these exotic magnetic atoms. However, the nature and distribution of resonances for these two systems are completely different. Feshbach resonances in s -wave collisions of magnetic atoms are anisotropy-induced due to a coupling to rotating molecular states containing energetically higher Zeeman sublevels. The long-range magnetic dipole-dipole and electrostatic interactions are the main source of this anisotropy. This is in stark contrast to the alkali-metals, where the strongest resonances are hyperfine-induced at short range and due to resonant bound states that do not rotate.

In this review we also emphasized a new way of looking at and describing interactions between atoms and molecules with a multiplicity of internal states. This approach involved the statistical analyses of Feshbach resonance distribution using random matrix theory. The analysis of the resonance distribution of experimentally observed Feshbach spectra as well as theoretical spectra from quantum-mechanical

scattering calculations in erbium could be satisfactorily classified in terms of random matrix theory.

Finally, we speculate that there is a growing interest in the creation of samples of trapped ultracold mixtures of highly magnetic lanthanide and alkali-metal atoms. These mixtures may have lower collisional anisotropy and produce less complex resonance spectra, possibly leading to a more easily controllable system.

Acknowledgments

The author thanks Dr E Tiesinga, Dr A Petrov and Professor F Ferlaino for fruitful discussions of the various topics of this review. We acknowledge support by the Air-Force Office of Scientific Research and the National Science Foundation of the USA.

References

- [1] Griesmaier A, Werner J, Hensler S, Stuhler J and Pfau T 2005 Bose-Einstein condensation of chromium *Phys. Rev. Lett.* **94** 160401
- [2] Lu M, Burdick N Q, Ho S and Lev B L 2011 Strongly dipolar Bose-Einstein condensate of dysprosium *Phys. Rev. Lett.* **107** 190401
- [3] Lu M, Burdick N Q and Lev B L 2012 Quantum degenerate dipolar Fermi gas *Phys. Rev. Lett.* **108** 215301
- [4] Frisch A, Aikawa K, Mark M, Rietzler A, Schindler J, Zupanic E, Grimm R and Ferlaino F 2012 Narrow-line magneto-optical trap for erbium *Phys. Rev. A* **85** 051401(R)
- [5] Aikawa K, Frisch A, Mark M, Baier S, Rietzler A, Grimm R and Ferlaino F 2012 Bose-Einstein condensation of erbium *Phys. Rev. Lett.* **108** 210401
- [6] Kato S, Sugawa S, Shibata K, Yamamoto R and Takahashi Y 2013 Resonant control of interactions between different electronic states *Phys. Rev. Lett.* **110** 173201
- [7] Khramov A, Hansen A, Dowd W, Roy R J, Makrides C, Petrov A, Kotochigova S and Gupta S 2014 Ultracold heteronuclear mixture of ground and excited state atoms *Phys. Rev. Lett.* **112** 033201
- [8] Fregoso B M and Fradkin E 2009 Ferronematic ground state of the dilute dipolar Fermi gas *Phys. Rev. Lett.* **103** 205301
- [9] Fregoso B M, Sun K, Fradkin E, and Lev B L 2009 Biaxial nematic phases in ultracold dipolar Fermi gases *New J. Phys.* **11** 103003
- [10] de Paz A, Sharma A C A, Maréchal E, Huckans J H, Pedri P, Santos L, Gorceix O, Vernac L and Laburthe-Tolra B 2013 Non-equilibrium quantum magnetism in a dipolar lattice gas *Phys. Rev. Lett.* **111** 185305
- [11] Budker D, DeMille D and Commins E D 1994 Experimental investigation of excited states in atomic dysprosium *Phys. Rev. A* **50** 132-43
- [12] Nguyen A T, Budker D, DeMille D and Zolotarev M 1997 Search for parity nonconservation in atomic dysprosium *Phys. Rev. A* **56** 3453-63
- [13] Derevianko A and Cannon C C 2004 Quantum computing with magnetically interacting atoms *Phys. Rev. A* **70** 062319
- [14] Rable P, DeMille D, Doyle J M, Lukin M D, Schoelkopf R J and Zoller P 2006 Hybrid quantum processors: molecular ensembles as quantum memory for solid state circuits *Phys. Rev. Lett.* **97** 033003
- [15] Fano U 1966 Effects of configuration interaction on intensities and phase shifts *Phys. Rev.* **124** 1866
- [16] Moerdijk A J, Verhaar B J and Axelsson A 1995 Resonances in ultracold collisions of ${}^6\text{Li}$, ${}^7\text{Li}$ and ${}^{23}\text{Na}$ *Phys. Rev. A* **51** 4852-61

- [17] Köhler T, Góral K and Julienne P 2006 Production of cold molecules via magnetically tunable Feshbach resonances *Rev. Mod. Phys.* **78** 1311
- [18] Ni K-K, Ospelkaus S, de Miranda M H G, Pe'er A, Neyenhuis B, Zirbel J J, Kotochigova S, Julienne P S, Jin D S and Ye J 2008 A high phase-space-density gas of polar molecules in the rovibrational ground state *Science* **322** 231
- [19] Danz J G, Haller E, Gustavsson M, Mark M J, Hart R, Bouloufa N, Dulieu O, Ritsch H and Nägerl H-C 2008 Quantum gas of deeply bound ground state molecules *Science* **321** 1062–6
- [20] Kraemer T, Mark M, Waldburger P, Danzl J G, Chin C, Engeser B, Lange A D, Pilch P, Jaakkola A, Nägerl H-C and Grimm R 2006 Evidence for Efimov quantum states in an ultracold gas of caesium atoms *Nature* **440** 315
- [21] Tiesinga E, Verhaar B J and Stoof H T C 1993 Threshold and resonance phenomena in ultracold ground-state collisions *Phys. Rev. A* **47** 4114
- [22] Inoué S, Andrews M R, Stenger J, Miesner H-J, Stamper-Kurn D M and Ketterle W 1998 Observation of Feshbach resonances in a Bose–Einstein condensate *Nature* **392** 151–4
- [23] Chin C, Grimm R, Julienne P S and Tiesinga E 2010 Feshbach resonances in ultracold gases *Rev. Mod. Phys.* **82** 1225
- [24] Lahaye T, Menotti C, Santos L, Lewenstein M and Pfau T 2009 The physics of dipolar bosonic quantum gases *Rep. Prog. Phys.* **72** 126401
- [25] Stuhler J, Griesmaier A, Koch T, Fattori M, Pfau T, Giovanazzi S, Pedri P and Santos L 2005 Observation of dipole–dipole interaction in a degenerate quantum gas *Phys. Rev. Lett.* **95** 150406
- [26] Krems R V, Groenenboom G C and Dalgarno A 2004 Electronic interaction anisotropy between atoms in arbitrary angular momentum states *J. Phys. Chem. A* **108** 8941–8
- [27] Lu M-J, Singh V and Weinstein D 2009 Inelastic titanium–titanium collisions *Phys. Rev. A* **79** 050702(R)
- [28] Connolly C B, Au Y S, Doret C, Ketterle W and Doyle J M 2010 Large spin relaxation rates in trapped submerged-shell atoms *Phys. Rev. A* **81** 010702
- [29] Hensler S, Werner J, Griesmaier A, Schmidt P O, Görlitz A, Pfau T, Giovanazzi S and Rzażewski K 2003 Dipolar relaxation in an ultra-cold gas of magnetically trapped chromium atoms *Appl. Phys. B* **77** 765–72
- [30] Hancox C I, Doret S C, Hummon M T, Luo L and Doyle J M 2004 Magnetic trapping of rare-earth atoms at millikelvin temperatures *Nature* **431** 281–4
- [31] Lu M, Youn S H and Lev B 2010 Trapping ultracold dysprosium: a highly magnetic gas for dipolar physics *Phys. Rev. Lett.* **104** 063001
- [32] Kotochigova S and Petrov A 2011 Anisotropy in the interaction of ultracold dysprosium *Phys. Chem. Chem. Phys.* **13** 19165
- [33] Wigner E P 1951 On a class of analytic functions from the quantum theory of collisions *Ann. Math. Second Ser.* **53** 36
- [34] Dyson F J and Mehta M L 1963 Statistical theory of the energy levels of complex systems. IV *J. Math. Phys.* **4** 701
- [35] Bohigas O, Giannoni M J and Schmit C 1984 Characterization of chaotic quantum spectra and universality of level characterization of chaotic quantum spectra and universality of level fluctuation laws *Phys. Rev. Lett.* **52** 1
- [36] Petrov A, Tiesinga E and Kotochigova S 2012 Anisotropy-induced Feshbach resonances in a quantum dipolar gas of highly magnetic atoms *Phys. Rev. Lett.* **109** 103002
- [37] Kokouline V, Santra R and Greene C H 2003 Multichannel cold collisions between metastable Sr atoms *Phys. Rev. Lett.* **90** 253201
- [38] Frisch A, Mark M, Aikawa K, Ferlaino F, Bohn J L, Makrides C, Petrov A and Kotochigova S 2014 Quantum chaos in ultracold collisions of gas-phase erbium atoms *Nature* **507** 475–9
- [39] Kramida A, Ralchenko Yu, Reader J and NIST ASD team NIST Atomic Spectra Database (ver. 5.0) <http://physics.nist.gov/asd>
- [40] Lawler J E, Wyart J and Hartog E A D 2010 Atomic transition probabilities of Er *J. Phys. B: At. Mol. Opt. Phys.* **43** 235001
- [41] Werner J, Griesmaier A, Hensler S, Stuhler J, Pfau T, Simoni A, and Tiesinga E 2005 Observation of Feshbach resonances in an ultracold gas of ^{52}Cr *Phys. Rev. Lett.* **94** 183201
- [42] Pavlović Z, Krems R V, Côté R and Sadeghpour H R 2005 Magnetic Feshbach resonances, Zeeman relaxation in bosonic chromium gas with anisotropic interaction *Phys. Rev. A* **71** 061402(R)
- [43] Stuhler J, Griesmaier A, Werner J, Koch T, Fattori M and Pfau T 2010 Ultracold chromium atoms: from Feshbach resonances to a dipolar Bose–Einstein condensate *J. Mod. Opt.* **54** 647–60
- [44] Lahaye T, Koch T, Fröhlich B, Fattori M, Metz J, Griesmaier A, Giovanazzi S and Pfau T 2007 Strong dipolar effects in a quantum ferrofluid *Nature* **448** 672–5
- [45] Koch T, Lahaye T, Metz J, Fröhlich B, Griesmaier A and Pfau T 2008 Stabilizing a purely dipolar quantum gas against collapse *Nature Phys.* **4** 218
- [46] Lahaye T, Metz J, Fröhlich B, Koch T, Meister M, Griesmaier A, Pfau T, Saito H, Kawaguchi Y and Ueda M 2008 d-wave collapse and explosion of a dipolar Bose–Einstein condensation of chromium *Phys. Rev. Lett.* **101** 080401
- [47] Pasquiou B, Bismut G, Beaufiles Q, Crubellier A, Maréchal E, Pedri P, Vernac L, Gorceix O and Laburthe-Tolra B 2010 Control of dipolar relaxation in external fields *Phys. Rev. A* **81** 042716
- [48] Pasquiou B, Bismut G, Maréchal E, Pedri P, Vernac L, Gorceix O and Laburthe-Tolra B 2011 Spin relaxation and band excitation of the dipolar Bose–Einstein condensate in 2D optical lattice *Phys. Rev. Lett.* **106** 015301
- [49] Pasquiou B, Maréchal E, Bismut G, Pedri P, Vernac L, Gorceix O and Laburthe-Tolra B 2011 Spontaneous demagnetization of a dipolar spinor Bose gas in an ultralow magnetic field *Phys. Rev. Lett.* **106** 255303
- [50] Müller S, Billy J, Henn E A L, Kadau H, Griesmaier A, Jona-Lasinio M, Santos L and Pfau T 2011 Stability of a dipolar Bose–Einstein condensate in a one-dimensional lattice *Phys. Rev. A* **84** 053601
- [51] Billy J, Henn E A L, Müller S, Maier T, Kadau H, Griesmaier A, Jona-Lasinio M, Santos L and Pfau T 2012 Deconfinement-induced collapse of a coherent array of dipolar Bose–Einstein condensates *Phys. Rev. A* **86** 051603(R)
- [52] Hensler S, Greiner A, Stuhler J and Pfau T 2005 Depolarisation cooling of an atomic cloud *Europhys. Lett.* **71** 918–24
- [53] Fattori M, Koch T, Goetz S, Griesmaier A, Hensler S, Stuhler J and Pfau T 2006 Demagnetization cooling of a gas *Nature Phys.* **2** 765–8
- [54] Volchkov V V, Rührig J, Pfau T and Griesmaier A 2014 Efficient demagnetization cooling of atoms and its limits *Phys. Rev. A* **89** 043417
- [55] Santos L and Pfau T 2006 Spin-3 chromium Bose–Einstein condensates *Phys. Rev. Lett.* **96** 190404
- [56] Santos L, Fattori M, Stuhler J and Pfau T 2007 Spinor condensates with a laser-induced quadratic Zeeman effect *Phys. Rev. A* **75** 053606
- [57] Kawaguchi Y, Saito H and Ueda M 2006 Can spinor dipolar effects be observed in Bose–Einstein condensates? *Phys. Rev. Lett.* **98** 110406
- [58] Hancox C I, Doret S C, Hummon M T, Krems R V and Doyle J M 2005 Suppression of angular momentum transfer

- in cold collisions of transition metal atoms in ground states with nonzero orbital angular momentum *Phys. Rev. Lett.* **94** 013201
- [59] KREMS R V, KLOS J, RODE M F, SZCZESNIAK M M, CHALASIŃSKI G and DALGARNO A 2005 Suppression of angular forces in collisions of non-s-state transition metal atoms *Phys. Rev. Lett.* **94** 013202
- [60] HARRIS J G E, NGUYEN S, DORET S C, KETTERLE W and DOYLE J M 2007 Spin-exchange collisions of submerged shell atoms below 1 kelvin *Phys. Rev. Lett.* **99** 223201
- [61] TSCHERBUL T V, BUCHACHENKO A A, DALGARNO A, LU M-J and WEINSTEIN J D 2009 Suppression of Zeeman relaxation in cold collisions of $^2p_{1/2}$ atoms *Phys. Rev. A* **80** 040701(R)
- [62] KREMS R V and BUCHACHENKO A A 2005 Electronic interaction anisotropy between open-shell lanthanide atoms and helium from cold collision experiment *J. Chem. Phys.* **123** 101101
- [63] SANTRA R and GREENE C H 2003 Tensorial analysis of the long-range interaction between metastable alkaline-earth-metal atoms *Phys. Rev. A* **67** 062713
- [64] GROENENBOOM G C, CHU X and KREMS R V 2007 Electronic anisotropy between open shell atoms in first and second order perturbation theory *J. Chem. Phys.* **126** 204306
- [65] MIES F H 1984 A multichannel quantum defect analysis of diatomic predissociation, inelastic atomic scattering *J. Chem. Phys.* **80** 2514–25
- [66] JULIENNE P S and MIES F H 1989 Collisions of ultracold trapped atoms *J. Opt. Soc. Am. B* **6** 2257–69
- [67] BAUMANN K, BURDICK N Q, LU M and LEV B L 2014 Observation of low-field Fano–Feshbach resonances in ultracold gases of dysprosium *Phys. Rev. A* **89** 020701(R)
- [68] MCCLELLAND J J and HANSEN J L 2006 Laser cooling without repumping: a magneto-optical trap for erbium atoms *Phys. Rev. Lett.* **96** 143005
- [69] AIKAWA K, FRISCH A, MARK M, BAIER S, GRIMM R and FERLAINO F 2014 Reaching Fermi degeneracy via universal dipolar scattering *Phys. Rev. Lett.* **112** 010404
- [70] TICKNOR C 2008 Collisional control of ground state polar molecules and universal dipolar scattering *Phys. Rev. Lett.* **100** 133202
- [71] BOHN J L, CAVAGNERO M and TICKNOR C 2009 Quasiuniversal dipolar scattering in cold and ultracold gases *New J. Phys.* **11** 055039
- [72] YAMAGUCHI A, UETAKE S, HASHIMOTO D, DOYLE J M and TAKAHASHI Y 2008 Inelastic collisions in optically trapped ultracold metastable ytterbium *Phys. Rev. Lett.* **101** 233002
- [73] YAMAGUCHI A, UETAKE S, KATO S, ITO H, and TAKAHASHI Y 2010 High-resolution laser spectroscopy of a Bose–Einstein condensate using the ultranarrow magnetic quadrupole transition *New J. Phys.* **12** 103001
- [74] HARA H, KONISHI H, NAKAJIMA S, TAKASU Y and TAKAHASHI Y 2013 A three-dimensional optical lattice of Ytterbium and Lithium atomic mixture *J. Phys. Soc. Jpn* **83** 014003
- [75] REID R H G and DALGARNO A 1969 Fine-structure transitions and shape resonances *Phys. Rev. Lett.* **22** 1029
- [76] MIES F H 1973 Molecular theory of atomic collisions: fine structure transitions *Phys. Rev. A* **7** 942
- [77] ALEXANDER M H, ORLIKOWSKI T, and STRAUB J E 1983 Theoretical study of intramultiplet transitions in collisions of atoms in 3p electronic states with structureless targets: $\text{Ca}(^3p) + \text{He}$ *Phys. Rev. A* **28** 73
- [78] AQUILANTI V, CANDORI R and PIRANI F 1988 Molecular beam studies of weak interactions for open-shell systems: the ground and lowest states of rare gas oxides *J. Chem. Phys.* **89** 6157
- [79] ZYGELMAN B, DALGARNO A and SHARMA R D 1994 Excitation of the $^3p_{J=0,1,2}$ fine-structure levels of atomic oxygen in collisions with oxygen atoms *Phys. Rev. A* **50** 3920
- [80] MAXWELL S E, HUMMON M T, WANG Y, BUCHACHENKO A A, KREMS R V and DOYLE J M 2008 Spin–orbit interaction and large inelastic rates in Bismuth–helium collisions *Phys. Rev. A* **78** 042706
- [81] DUBERNET M-L and HUTSON J M 1994 Atom–molecule van der Waals complexes containing open-shell atoms: I. General theory and bending levels *J. Chem. Phys.* **101** 1939
- [82] DUBERNET M-L and HUTSON J M 1994 Atom–molecule van der Waals complexes containing open-shell atoms: II. The bound states of Cl–HCl *J. Phys. Chem.* **98** 5844
- [83] HANSEN A H, KHRAMOV A, DOWD W H, JAMISON A O, IVANOV V V and GUPTA S 2011 Quantum degenerate mixture of ytterbium, lithium atoms *Phys. Rev. A* **84** 011606(R)
- [84] BRUE D and HUTSON J M 2012 Magnetically tunable Feshbach resonances in ultracold Li–Yb mixtures *Phys. Rev. Lett.* **108** 043201
- [85] GONZALEZ-MARTINEZ M L and HUTSON J M 2013 Magnetically tunable Feshbach resonances in $\text{Li+Yb}(^3P_J)$ *Phys. Rev. A* **88** 020701(R)